Equilibrium Exchange Processes of the Aqueous Tryptophan Dipeptide

Sayan Bagchi, Adam K. Charnley, Amos B. Smith III, and Robin M. Hochstrasser*

Department of Chemistry, University of Pennsylvania, Philadelphia, Pennsylvania 19104-6323

Received: December 18, 2008; Revised Manuscript Received: April 9, 2009

The tryptophan dipeptide (NATMA) in D_2O shows two conformers having distinctive acetyl end amide-I′ transition frequencies. In 2D echo spectroscopy, cross peaks between these conformer transitions are used to show that they are undergoing exchange on the 1.5 ps time scale. Simulations suggest that the accessibility of the amide group to water is restricted in one of the conformations.

1. Introduction

The elementary chemical bond scale motions of small peptides underpin the dynamics of the backbone structures of more complex protein systems, so they have an important role in protein stability and function. The relevant potential energy functions of small peptides range from well-defined conformational minima separated by large barriers to energy surfaces linking structures through many small barriers. Molecular dynamics (MD) simulations have predicted ultrafast equilibrium transitions between conformers connected by small activation barriers in small peptides. A low activation barrier of 2.5 kcal/mol has been calculated for the picosecond conversion of C_{7eq} to the C_5 conformer of the alanine dipeptide.[1,2] Similar calculations of activation energy barriers and prediction of the interconversion rates have been extended to the tripeptides of alanine[2] and glycine.[3] Hexapeptides[2,3] have been predicted to interconvert between sheet and helical structures, which are the most prominent structural elements of the protein backbone. The present knowledge regarding ultrafast equilibrium conformational dynamics of small peptides stems mainly from MD simulations notwithstanding many experimental studies of conformational motions near equilibrium occurring on microsecond-to-nanosecond time scales by NMR[4,5] and ESR[6] and laser-induced pH and temperature-jump experiments.[7,8] Ultrafast processes under nonequilibrium conditions have been reported for basic peptide motions using molecular photoswitches.[9−12] Although MD simulations have predicted the importance of ultrafast elementary steps in structure evolution for biological activity[13] and selectivity,[14] the experimental manifestation of picosecond time scale interchanges of distinct peptide conformers at equilibrium, as reported in the current study, is unique.

Recently, the 2D IR spectroscopic method has been used to measure the kinetics of picosecond chemical processes at equilibrium in cases where the interchanging populations have distinct mean vibrational frequencies.[15−17]The intrinsic fast temporal resolution of the 2D IR technique thereby extends the accessible range of equilibrium dynamics into the femtosecond/picosecond regime.[18] This experimental strategy has been employed to measure dynamic processes such as methanol hydrogen bonding to amide-I′ modes,[19] hydrogen-bond kinetics of nitriles,[15,20] complexation,[16] single-bond rotations,[21] and fluctionality.[17] These concepts are applied to aqueous peptide dynamics in the present work.

Spectroscopic investigations of *N*-acetyl tryptophan methyl amide (NATMA; tryptophan dipeptide or Trp-dipeptide) as an isolated molecule in the gas phase have demonstrated the existence of many conformational minima.[22−24] In the gas phase the lowest energy C_5 and C_7 structures were found to be isoenergetic despite the significant differences in the peptide backbone configurations and presumed large activation barriers connecting them. Previous solution phase experimental results have shown that the tryptophan dipeptide structures are solvent sensitive, ranging from those of the most prevalent gas phase forms in nonpolar solvents to extended hydrogen-bonded structures in water.[25] It has been suggested[25] that multiple hydrogen-bonded configurations that interchange on the picosecond time scale are present for the tryptophan dipeptide in methanol; however, the conformational dynamics in the more relevant aqueous environment has not been previously reported. Recent simulations of vibrational spectra of polypeptides have predicted that the water structures near the amide carbonyls are modified by hydrophobic residues, such as tryptophan.[26] The tryptophan dipeptide, with its two amide-I′ modes whose time-dependent vibrational frequency distributions can be separately examined, is used here as a model of the hydrophobic protection effects of the tryptophan residue on the water structural dynamics.[27,28] The amide-I′ carbonyl of its *N*-methylamino end is substituted with $^{13}C{=}^{16}O$ to distinguish it spectrally from the amide-I′ transitions of the acetyl end of the peptide where the dynamics occurs. The results concern the dynamics of the amide-I′ vibrational frequency distributions and simulations of how the indole ring of tryptophan and the hydrogen-bond dynamics of water around the carbonyl group are changing in the equilibrium dynamics.

2. Materials and Methods

Tryptophan Dipeptide. The method of preparation and purification of *N*-acetyl tryptophan methyl amide has been described elsewhere.[25,29] A sample in D_2O (56 μm path length CaF_2 cell) having an optical density of 0.03 for the *N*-methylamino end amide-I′ peak was used in the experiments.

2D IR Spectra. Heterodyned spectral interferometry was employed using the laser arrangement described previously.[30,31] Fourier-transform limited 75 fs pulses were used in the 2D IR experiments. Three of these pulses, each with energy of 400 nJ and wave vectors k_1, k_2, and k_3, were incident on the sample. The phase-matched signal at wave vector $-k_1 + k_2 + k_3$ was detected by heterodyning it with a local oscillator pulse that always preceded the signal pulse by a fixed interval of 1.5 ps.

* Corresponding author. Tel: 215-898-8203. Fax: 215-898-0590. E-mail: hochstra@sas.upenn.edu.

10.1021/jp811168x CCC: $40.75
Published on Web 05/21/2009

The interval between pulses 1 and 2 is denoted as the coherence time τ, between pulses 2 and 3 is denoted as the population or waiting period T, and between pulse 3 and the detected signal is denoted as t. The rephasing and nonrephasing sequences correspond to k_1 arriving earlier or later than k_2, respectively. The signal and local oscillator pulses were combined at the focal plane of a monochromator having a 64-element mercury−cadmium−telluride array detector (InfraRed Associates, Stuart, FL). Each detector element is 200 μm in width and 1 mm in height. The raw data collected by using this method were in the form of a 2D array of coherence time τ (in 2 fs steps from −3 to 3 ps) and detected wavelength (in ∼15 nm steps.) To obtain absorptive or correlation spectra, rephasing and nonrephasing 2D frequency spectra were added. Details of the 2D IR data processing have been described previously.[32,33] The 2D spectral function $\tilde{S}$ (ω_τ, ω_t, T) for each population interval T depends on the coherence and detection frequencies ω_τ and ω_t. The method of obtaining the ratio of the diagonal and cross-peak volumes at different waiting times is discussed in more detail below.

Molecular Mechanics Calculations. Molecular mechanics calculations of the tryptophan dipeptide were carried out using the CHARMM force field in HyperChem.[34] The extended solvent hydrogen-bonded structure of the tryptophan in D_2O with Ramachandran angles of ($\pm$160 $\pm$10°, $\pm$75 $\pm$10°)[25] was used as the initial backbone geometry. A conformational search based on single point calculations, which provided the value for the total potential energy at each point, was performed by separately varying the $C_\alpha-C_\beta$ and $C_\beta-C_\gamma$ bond rotations from −180° to 180° with a step size of 5° (a positive value denotes a clockwise rotation of the bond). The $C_\alpha-C_\beta$ bond rotation is defined by the change in the dihedral angle formed by the *N*-methylamino end carbonyl carbon atom C_{am} and C_α, C_β, and C_γ. The $C_\beta-C_\gamma$ bond rotation is defined by the change in the dihedral angle formed by the atoms C_α, C_β, and C_γ and the indole ring carbon atom 9 connected to C_γ. The potential energy surface obtained from the conformational search predicted two lowest-energy minima separated by 3 kcal mol^{-1}: one with the indole ring oriented toward the acetyl end ($C_\alpha-C_\beta$ and $C_\beta-C_\gamma$ bond rotations are 120° and 145°) and the other with the indole ring oriented toward the *N*-methylamino end ($C_\alpha-C_\beta$ and $C_\beta-C_\gamma$ bond rotations are 45° and 60°). Geometry optimization of these two conformational minima was performed using the steepest descent algorithm, and they converged to a gradient of less than 0.001 kcal mol^{-1} Å^{-1}.

Molecular Dynamics Simulations. The MD simulations in explicit solvent water (H_2O) have been carried out using the NAMD2.5 package.[35] The initial structures used for the MD simulations were either of the energy-minimized structures obtained from the above-mentioned molecular mechanics calculations. Both lead to the same equilibrated distribution. Structures showing the extremes of the $C_\alpha-C_\beta$ bond rotation from this distribution are shown in Figure 1. The MD simulations include 1752 explicit water molecules of the TIP3P type in a cubic box (30 Å). The CHARMM27 force field[36] was used to compute all interactions. A cutoff of 12 Å was used for the nonbonded interactions. The long-range electrostatic interaction was evaluated by the Ewald sum approach.[37] The system was initially energy minimized and equilibrated at 300 K for 1 ns at a time step of 2 fs. The simulations were performed for constant NPT condition at a time step of 2 fs for 2 ns, and 10 000 evenly distributed snapshots were used for further analysis of the simulation trajectories. Throughout this paper no distinction is made between H_2O and D_2O. The simulations were all carried out in H_2O, but the experiments are all in D_2O.

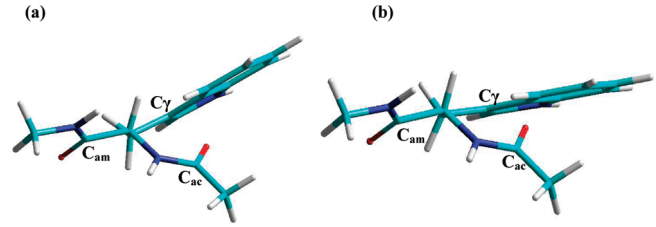

Figure 1. Structures of the tryptophan dipeptide. Newman projections of two of the structures of the tryptophan dipeptide looking down the $C_\alpha-C_\beta$ bonds. (a) and (b) represent the extremes of the $C_\alpha-C_\beta$ bond rotation found from the molecular dynamics simulations.

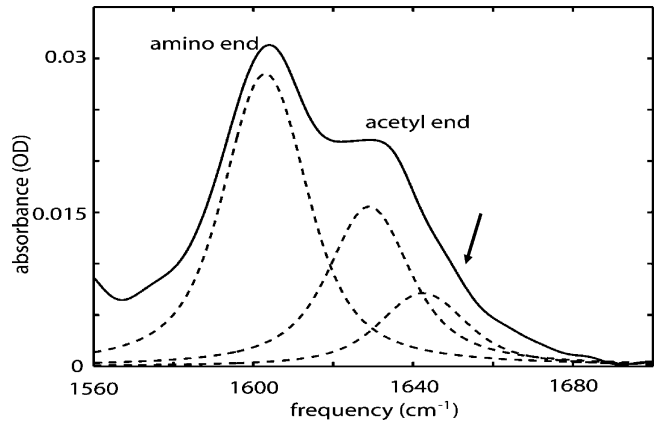

Figure 2. FTIR spectrum of tryptophan dipeptide in D_2O. The FTIR spectrum in D_2O of the tryptophan dipeptide amide-I′ bands is labeled with $^{13}C{=}^{16}O$ at the amino end. The weaker underlying transition at the acetyl end is indicated by the arrow. The dashed lines are the fitted Voigt profile components.

3. Experimental Results

The FTIR spectrum of the isotopically labeled tryptophan dipeptide in D_2O (see Figure 2) showed two separated amide-I′ bands with the *N*-methylamino ($^{13}C{=}^{16}O$) end transition frequency at 1605 cm^{-1} and the acetyl end ($^{12}C{=}^{16}O$) transition frequency at 1630 cm^{-1}. The band that peaked at 1630 cm^{-1} shows a shoulder near 1645 cm^{-1} that is marked by an arrow in Figure 2. A fit of the asymmetric band near 1630 cm^{-1} to two Voigt profiles yields bands at 1630 (fwhm = 24 cm^{-1}) and 1643 cm^{-1} (fwhm = 25 cm^{-1}), with the former having twice the cross section of the latter. The ratio of the cross sections of the *N*-methylamino end to the total acetyl end amide-I′ bands is 1.5.

The 2D IR spectra of the whole amide-I′ region shown in Figure 3a−d consist of the $v = 0 \rightarrow v = 1$ amide-I′ transitions on the diagonal and the $v = 1 \rightarrow v = 2$ transitions shifted along the horizontal axis (ω_t) by the diagonal anharmonicity of ca. 17 cm^{-1}.[25] The acetyl end amide-I′ mode region consists of two clearly separated transitions at 1630 and 1643 cm^{-1}. The resolved diagonal peak at $\omega_\tau = \omega_t$ = 1643 cm^{-1} corresponds to the shoulder seen in FTIR. The comparison of the FTIR and 2D IR spectra in this region presents another example of the advantage of 2D IR in separating closely spaced transitions. At zero waiting time, the higher-frequency acetyl end transition at ∼1643 cm^{-1} has 65% of the peak signal amplitude of the transition at ∼1630 cm^{-1}. This result is consistent with the computations of the 2D IR spectra based on the Voigt profile parameters from FTIR fitting and the standard response func-

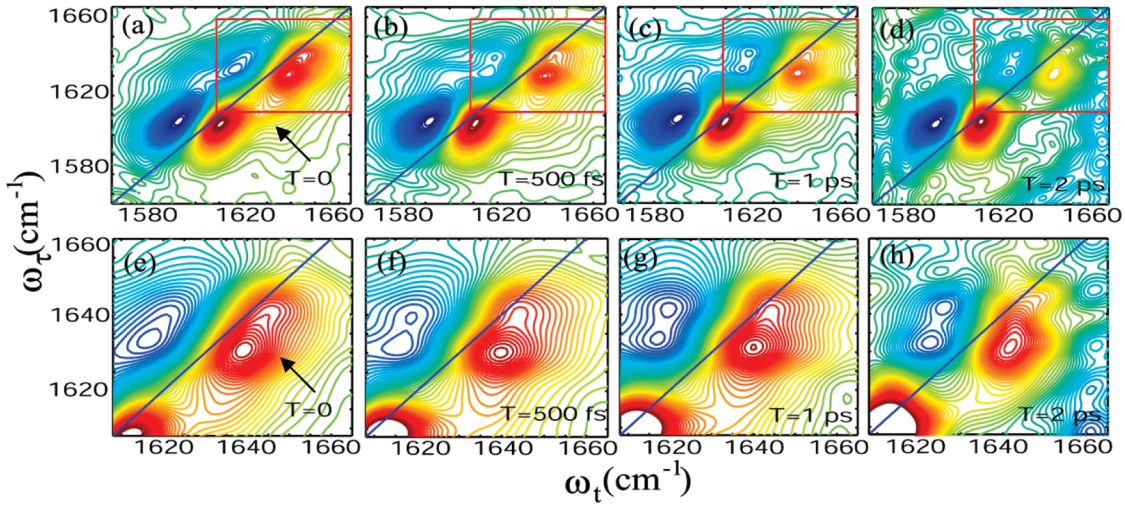

Figure 3. 2D IR spectra of tryptophan dipeptide in D_2O. Absorptive 2D IR spectrum at (a) $T = 0$, (b) $T = 500$ fs, (c) $T = 1$ ps, and (d) $T = 2$ ps. Enlargement of the frequency region of the acetyl end amide-I′ mode marked by the red boxes in panels a−d is shown in panels e−h.

tions[38] neglecting any exchange kinetics as will be the situation at waiting time $T = 0$.[25] As the temperature is increased to 60 °C, the fractional amplitude at 1643 cm^{-1} increases to 94%. In contrast, the 2D IR spectra of the amide-I′ mode of the *N*-methylamino end shows a single peak elongated along the diagonal indicative of static inhomogeneous broadening. This is again consistent with the FTIR spectrum, which shows a single symmetric peak at 1605 cm^{-1}. In 2D IR, the *N*-methylamino end amide-I′ mode signal amplitude at 1605 cm^{-1} is larger than the combined acetyl end transitions. They are not expected to have identical spectral parameters since they are chemically distinct modes from MeCONH- and MeNHCO-. The signal amplitude of the diagonal peak at 1630 cm^{-1} is 70% of that of the peak at 1605 cm^{-1}.

Cross peaks between the amide-I′ transitions of the acetyl and *N*-methylamino ends could be identified at $T = 0$ (marked by an arrow in Figure 3a). The anharmonically shifted peaks of the acetyl end carbonyl interfere with the intermode cross peaks, which cause distortion and diminution of the signal amplitude in the $v = 1 \rightarrow v = 2$ region.[25] The waiting time dependence of the 2D IR spectra in D_2O at a selection of T is shown in Figure 3a−d. The change in peak shape at the cross-peak region of the acetyl end modes ($\omega_\tau = 1630$ cm^{-1}, $\omega_t = 1643$ cm^{-1}) with population period increasing from $T = 0$ to $T = 2$ ps is shown in Figure 3e−h, which is an enlargement of the data in the upper part of the figure. These data manifest the evolution of a cross peak between the two $v = 0 \rightarrow v = 1$ acetyl end amide-I′ transitions (marked by an arrow in Figure 3e).

The cross peak at ($\omega_\tau = 1630$ cm^{-1}, $\omega_t = 1643$ cm^{-1}) evolves over the population time T range of 0−3.5 ps. A quantitative measure of the ratio of the integrated areas of the cross peak and the diagonal peak at 1630 cm^{-1} was obtained at different T by subtracting the 2D spectrum spectra $\tilde{S}(\omega_\tau, \omega_t, 0)$ at $T = 0$ from $\tilde{S}(\omega_\tau, \omega_t, T)$ at various T values. Through this method, the cross-peak signal could be isolated, integrated over the frequency space, and compared with the diagonal signal. The T dependence of the ratio of the cross peak and diagonal signals defined as $\tilde{S}_{AB}/\tilde{S}_{AA}$ (A and B are defined below) is plotted in Figure 4.

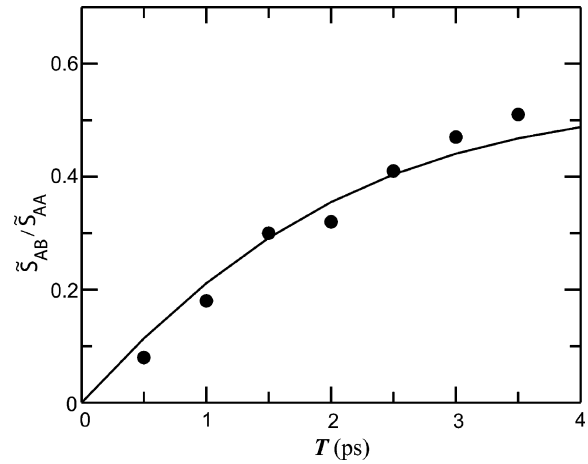

Figure 4. Conformational exchange kinetics of tryptophan dipeptide. Experimental values (solid circles) of $\tilde{S}_{AB}/\tilde{S}_{AA}$ as defined in the text. Waiting time evolution of the ratio $\tilde{S}_{AB}/\tilde{S}_{AA}$ as described by eq 2 (solid line).

4. Discussion

When a chemical or conformational process results in the interchange of populations of structures having different vibrational frequencies, the waiting time dependence of the 2D IR signal is affected in a predictable manner.[15,19,21] Chemical exchange causes the development of a signal in the region of the cross peaks between the interchanging states, while the two diagonal-peak signal regions are caused to diminish. Population relaxation causes all the signals to decrease in amplitude with increasing waiting time. An analysis of these changes yields the equilibrium kinetics on the picosecond time scale. A number of examples of such exchange have now been reported.[15−17,20,21]

In the present example, the multiple transitions of the acetyl end amide-I′ mode in the 2D IR spectra indicate the existence of two conformational distributions of tryptophan dipeptide in D_2O, each having a spectrally distinct vibrational peak, one at 1630 cm^{-1} (A) and the other at 1643 cm^{-1} (B). If there is an equilibrium between the conformational distributions, labeled A and B, with an equilibrium constant $K_{eq} = k_{AB}/k_{BA}$, then cross peaks between the vibrational transitions of these conformations will appear in the 2D IR spectra when the two conformers exchange, during the population period of the 2D IR sequence. The evolution of the cross peaks between the amide-I′ modes at 1643 and 1630 cm^{-1} indicates fast chemical exchange between the two conformational distributions.

A simplified kinetic model was constructed to analyze the exchange kinetics[15] in which it was assumed that the spectrum

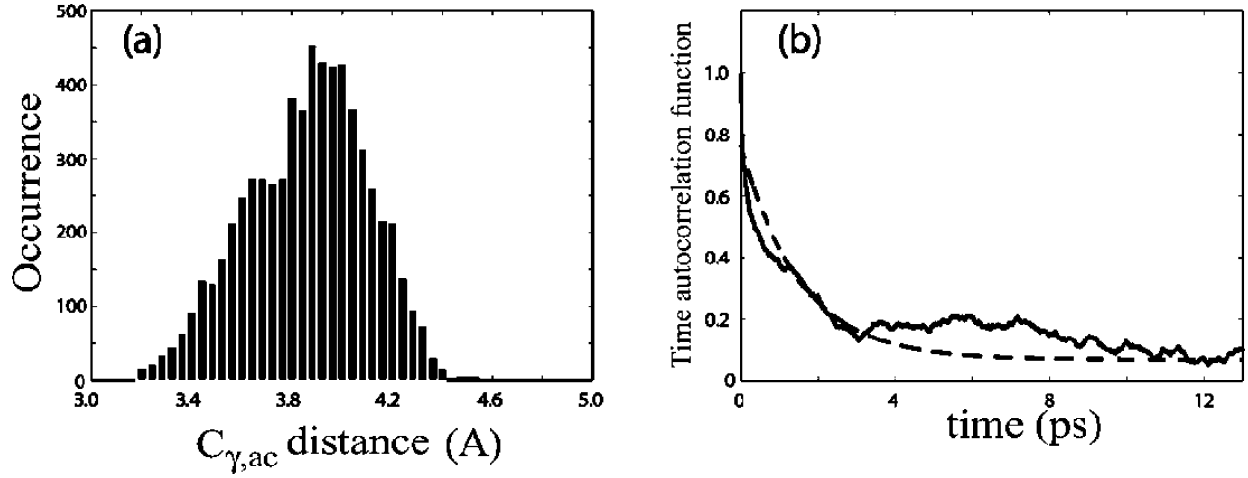

Figure 5. Simulation results. (a) Occurrence distribution of the distance $C_{\gamma,ac}$ between carbon atoms C_γ and C_{ac} from the MD simulation. (b) Simulated time autocorrelation function (solid) of the distance $C_{\gamma,ac}$ fitted to an exponential decay (dashed) with a time constant of 0.67 ps^{-1}.

of the acetyl end amide-I′ doublet corresponds to two exchanging states characterized by one relaxation time and an equilibrium constant. It will be shown below that these assumptions are consistent with a computation of the IR spectrum and molecular dynamics simulations. The two-state model is illustrated schematically as

$$\underset{\text{decay}}{\overset{T_{1A}}{\leftarrow}} \text{A}(1630\text{cm}^{-1}) \underset{k_{BA}}{\overset{k_{AB}}{\rightleftarrows}} \text{B}(1643\text{cm}^{-1}) \underset{\text{decay}}{\overset{T_{1B}}{\rightarrow}} \quad (1)$$

where the two conformers (A and B) can undergo chemical exchange with forward and backward rate constants k_{AB} and k_{BA}. The diagonal 2D IR signal $\tilde{S}_{AA}$, for the state A at a given point in the two-dimensional space, has the content $\mu_A^4 R_{AA}(\omega_\tau, \omega_t) P_{AA}(T) N_A^{eq}$ where $R_{AA}(\omega_\tau, \omega_t)$ is a 2D IR spectral shape factor arising from all the Liouville pathways[18,39] contributing at that point, and N_A^{eq} is the equilibrium number density of A. The cross-peak signal $\tilde{S}_{AB}$ in the same notation is $\mu_A^2 \mu_B^2 R_{AB}(\omega_\tau, \omega_t) P_{AB}(T) N_A^{eq}$. Each of these signals is associated with the relevant transition dipoles (μ_A and μ_B) and the conditional probabilities $P_{AA}(T)$, $P_{AB}(T)$, $P_{BA}(T)$, or $P_{BB}(T)$ arising from kinetic equations, where $P_{AB}(T)$ is the probability of measuring the B population after time T if the system started out in A. When $T_{1A} = T_{1B}$, the ratio of the diagonal- and cross-peak signal areas can be approximated by a simple function of the exchange rate:

$$\tilde{S}_{AB}/\tilde{S}_{AA} = \frac{\mu_B^2(1 - e^{-k_R T})}{\mu_A^2\left(\frac{1}{K_{eq}} + e^{-k_R T}\right)} \quad (2)$$

where $\tilde{S}_{AB}/\tilde{S}_{AA}$ corresponds to the ratio of the integrated signals of the intramode cross peak centered at ($\omega_\tau = 1630$ cm^{-1}, $\omega_t = 1643$ cm^{-1}) and the diagonal peak at 1630 cm^{-1}. The relaxation rate is $k_R = k_{AB} + k_{BA}$. Equation 2 is approximate in the sense it assumes that the diagonal and cross peaks can be separated experimentally and integrated over all frequencies. If that were the case, then the area ratio would be independent of the dephasing dynamics. In reality, the transitions overlap which, when combined with the variations of line shape with waiting time, led to the relaxation time result being uncertain to within ca. 10%. The population lifetimes (T_1) and the transition dipole moments of the two conformers were taken to be equal. The computed 2D IR spectra at various waiting times, using standard response functions, indicate that the T dependence of the acetyl end transitions is not arising from the different population times of the overlapping diagonal peaks. The ratio of the peak 2D IR spectral amplitudes of the two acetyl end transitions approaches unity at high temp = 60°. Therefore, it is assumed that it is the equilibrium constant that is approaching unity because of the small free-energy separation between the interconverting states. If this analysis is correct, then it implies that the transition dipole moments (μ_A and μ_B) are equal, which is what will now be assumed.

To obtain the ratio $\tilde{S}_{AB}/\tilde{S}_{AA}$ at different waiting times, the peak heights of the acetyl end amide-I′ band at 1630 cm^{-1} in the 2D spectra at various T values were normalized to that at $T = 0$. Then the 2D spectrum at $T = 0$ was subtracted from the normalized spectra. The cross-peak positions in these difference spectra were confirmed at each value of T to be within 2 cm^{-1} (along ω_τ and ω_t) of the expected cross-peak position based on the diagonal-peak positions. The integrated cross-peak signal was obtained by summing up all the contour values greater than one-half of the maximum cross-peak intensity. By fitting the observed ratio $\tilde{S}_{AB}/\tilde{S}_{AA}$ at different population periods (Figure 4) to the two-state exchange model (eq 1), the rate of the chemical exchange was found to be $k_R = (6.9 \pm 1.0) \times 10^{11}$ s^{-1}; the uncertainty of ca. 15% arises from a ca. 10% uncertainty (as mentioned above) in estimating the integrated cross-peak signal from the overlapping transitions. The knowledge of the equilibrium constant from the population ratio of the two frequency distributions (assuming $\mu_A = \mu_B$, and that they are both independent of frequency) yields the forward (k_{AB}) and backward (k_{BA}) rates to be 2.4×10^{11} and 4.5×10^{11} s^{-1}, respectively.

The MD simulations provided predictions of the solvent influence on the molecular structure and dynamics. The simulation shows that the dipeptide is undergoing significant single-bond rotational dynamics that alters the proximity of the acetyl end amide group and the indole ring. The dominant motions involve rotations of 20° around the $C_\alpha - C_\beta$ single bond and 9° about the $C_\beta - C_\gamma$ bond. The full range of sample structures falls within the staggered conformations with respect to these two single bonds. The two extreme structures are depicted in Figure 1. The probability distribution of the distance $C_{\gamma,ac}$ between C_γ and C_{ac} (the acetyl end carbonyl carbon; see Figure 1) shows a bimodal distribution centered around 3.6 and 4.0 Å as shown in Figure 5a. The distance $C_{\gamma,ac}$ is independent of the $C_\beta - C_\gamma$ bond rotation angle, and the distributions in the MD simulations in Figure 5a mainly result from the $C_\alpha - C_\beta$ single-bond rotation. The single-bond rotation around $C_\alpha - C_\beta$ makes the hydrophobic

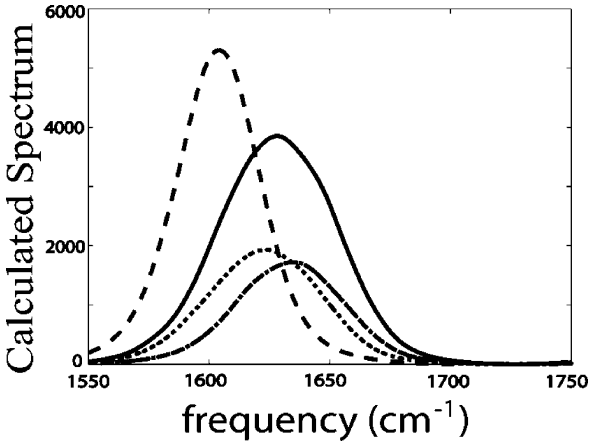

Figure 6. Calculated spectrum by SPECTRON[42] of the amide-I modes at the acetyl end (solid) and the *N*-acetylamino end (dashed). The spectrum of the acetyl end with at least two hydrogen bonds (dotted) and less than two hydrogen bonds (dashed dot).

indole ring become more proximate to the carbonyl carbon of the acetyl end in one of the conformational distributions centered at 4.0 Å. This configuration, corresponding to that in Figure 1b, is expected to modify the water (D_2O) structure around the acetyl amide unit as compared with the other conformer. An autocorrelation function of the simulated $C_{\gamma,ac}$ distance fluctuations, defined as $\langle \delta C_{\gamma,ac}(t) \delta C_{\gamma,ac}(0) \rangle$, was calculated by creating a binary distribution of the distance $C_{\gamma,ac}$ based on whether the distance is greater or less than 3.8 Å. The autocorrelation function of the binary distribution (see Figure 5b) decays with a time constant of 6.7×10^{11} s^{-1}, which is comparable with the experimentally obtained rate of chemical exchange. However, this connection does not explain the frequency shift between the two conformers.

The sensitivity of the amide-I′ modes to hydrogen bonding, resulting in a red-shift of the transition frequency for more strongly hydorgen-bonded structures, is well-known from the literature.[40,41] The frequency distributions of the amide-I modes, calculated from the MD trajectories using SPECTRON,[42] show a broad asymmetric distribution for the acetyl end and a narrower symmetric distribution for the *N*-methylamino end (as shown in Figure 6). This result shows that the two amide ends of the tryptophan dipeptide manifest the conformational distributions differently and have different environments in agreement with experiment. The simulation verifies that the proximity of the indole ring arising from the C−C single-bond rotation influences the hydrogen bonding of the water molecules to the acetyl end C═O and N−H. The hydrogen-bonding contributions from the different water structures associated with the acetyl amide were calculated from each of the MD snapshots. A water molecule was considered as hydrogen bonded to the acetyl end C═O (N−H) if R_{OO} (R_{ON}) < 3.5 Å and θ_{HOO} (θ_{HNO}) < 30°, where R_{OO} (R_{NO}) is the distance between the donor oxygen and acceptor oxygen (nitrogen) atoms and θ_{HOO} is the angle between the OH (NH) and OO (NO) vectors. The snapshots used in the SPECTRON[42] calculation were binned according to the number of hydrogen bonds based on the foregoing algorithm. Two spectra were computed: one with the acetyl amide unit forming two or more hydrogen bonds and the other with it forming less than two hydrogen bonds. These two spectra, both shown in Figure 6, add to yield the acetyl end asymmetric band. However, it is clear that the spectra with two or more hydrogen bonds (dotted line in Figure 6) are significantly down shifted (−10 cm^{-1}) from that with fewer than two hydrogen bonds. This analysis shows that the asymmetry in the calculated spectrum from SPECTRON[42] is arising from hydrogen-bond configurational differences. The ultrafast rotations around the single bonds cause alternating changes in the solvent (hydrogen-bonding) environment of the acetyl end amide group, giving rise to the two frequency distributions in the 2D spectra. The binning into fewer than two and two or more hydrogen bonds did not produce two bands having the experimental intensity ratio of 2:1, but it confirms the origin of the dual frequency distribution seen in the experiments.

To study further the effect of the disruption of the solvation at the acetyl carbonyl by the proximity of the hydrophobic indole ring, we studied the hydrogen-bond dynamics between the acetyl end C═O and the surrounding water molecules from the MD simulation trajectories by using the previously established method of estimating the time correlation functions.[43] The time correlation function $C_{HB}(t)$, given by the analytical form $\langle h(0)h(t) \rangle / \langle h^2 \rangle$,[43,44] was calculated from the MD simulation snapshots, where $h(t) = 1$ if one particular water molecule is hydrogen bonded (using the aforesaid algorithm) and $h(t) = 0$ if it is not. This procedure was repeated for all water molecules that formed hydrogen bonds during simulation. The simulated correlation function, which is the sum of the contributions from all of these water molecules, has an ultrafast component that decays in 100 fs, which is on the time scale predicted[45] for the librational motions of the water molecules. The correlation function $h(t)$ also decays on a time scale of 6.2×10^{11} s^{-1}, which describes the structural relaxation of the hydrogen bonds of the dipeptide. This rate is close to the measured exchange rate.

The results provide direct experimental evidence that the water structure and its dynamics in the neighborhood of an exposed amide unit depend significantly on the hydrophobic character of the nearby residue. It is likely that this factor will require consideration in descriptions of the dynamics of water near proteins, as already shown in some simulations.[46]

5. Conclusion

The acetyl end amide-I′ mode of the tryptophan dipeptide shows a double-peaked vibrational frequency distribution, indicating the existence of multiple conformers in D_2O. This spectral structure is more clearly resolved in 2D IR compared with FTIR. Cross peaks develop with increasing waiting time, indicating that the conformers are exchanging on the experimental time scale. A detailed study of the waiting time dependence and fitting based on the assumption there is exchange between only two states having equal transition dipoles evidence a relaxation time of 1.5 ps. MD simulations indicate that on the few picosecond time scale there is significant back and forth motion of the indole ring caused by axial rotations about the C−C single bonds. The C−C distance histogram is bimodal, suggesting there are two dominant states in the equilibrium structure distribution. The infrared spectrum of the acetyl end amide-I′ mode computed by SPECTRON[42] shows an asymmetry that is consistent with the presence of at least two peaks in the frequency distribution. The variations of the water structure around the carbonyl also track these molecular motions, suggesting that changes in the hydrogen-bond configurations cause the vibrational frequency shifts. In one group of conformations, the indole ring appears to offer more hydrophobic protection of the acetyl end carbonyl, which would result in the blue-shift of the vibrational frequency.

Acknowledgment. We thank Prof. S. Mukamel and his group for invaluable help with SPECTRON.[42] Discussion with Diego

Pantano is gratefully acknowledged. The research was supported by the NIH grant GM12592, by NSF, and by instrumentation through the Resource NIH P41 RR001348.

References and Notes

(1) Wei, D. Q.; Guo, H.; Salahub, D. R. *Phys. Rev. E: Stat., Nonlinear, Soft Matter Phys.* **2001**, *6401*, 011907.
(2) Solov'yov, I. A.; Yakubovich, A. V.; Solov'yov, A. V.; Greiner, W. *Phys. Rev. E: Stat., Nonlinear, Soft Matter Phys.* **2006**, *73*, 23–34.
(3) Yakubovich, A. V.; Solov'yov, I. A.; Solov'yov, A. V.; Greiner, W. *Eur. Phys. J. D* **2006**, *39*, 23–34.
(4) Dyson, H. J.; Wright, P. E. Elucidation of the protein folding landscape by NMR. In *Nuclear Magnetic Resonance of Biological Macromolecules, Part C*; Elsevier Academic Press Inc.: San Diego, CA, 2005; Vol. 394, p 299.
(5) Akke, M. *Curr. Opin. Struct. Biol.* **2002**, *12*, 642–647.
(6) Lietzow, M. A.; Hubbell, W. L. *Biophys. J.* **1998**, *74*, A278–A278.
(7) Williams, S.; Causgrove, T. P.; Gilmanshin, R.; Fang, K. S.; Callender, R. H.; Woodruff, W. H.; Dyer, R. B. *Biochemistry* **1996**, *35*, 691–697.
(8) Thompson, P. A.; Eaton, W. A.; Hofrichter, J. *Biochemistry* **1997**, *36*, 9200–9210.
(9) Bredenbeck, J.; Helbing, J.; Behrendt, R.; Renner, C.; Moroder, L.; Wachtveitl, J.; Hamm, P. *J. Phys. Chem. B* **2003**, *107*, 8654–8660.
(10) Bredenbeck, J.; Helbing, J.; Kolano, C.; Hamm, P. *ChemPhysChem* **2007**, *8*, 1747–1756.
(11) Bredenbeck, J.; Helbing, J.; Hamm, P. *J. Am. Chem. Soc.* **2004**, *126*, 990–991.
(12) Kolano, C.; Helbing, J.; Kozinski, M.; Sander, W.; Hamm, P. *Nature* **2006**, *444*, 469–472.
(13) Karplus, M.; Petsko, G. A. *Nature* **1990**, *347*, 631–639.
(14) Zhou, H. X.; Wlodek, S. T.; McCammon, J. A. *Proc. Natl. Acad. Sci. U.S.A.* **1998**, *95*, 9280–9283.
(15) Kim, Y. S.; Hochstrasser, R. M. *Proc. Natl. Acad. Sci. U.S.A.* **2005**, *102*, 11185–11190.
(16) Zheng, J.; Kwak, K.; Asbury, J.; Chen, X.; Piletic, I. R.; Fayer, M. D. *Science* **2005**, *309*, 1338–1343.
(17) Cahoon, J. F.; Sawyer, K. R.; Schlegel, J. P.; Harris, C. B. *Science* **2008**, *319*, 1820–1823.
(18) Sanda, F.; Mukamel, S. *J. Chem. Phys.* **2006**, *125*, 014507/1–12.
(19) Woutersen, S.; Mu, Y.; Stock, G.; Hamm, P. *Chem. Phys.* **2001**, *266*, 137–147.
(20) Kim, Y. S.; Hochstrasser, R. M. *J. Phys. Chem. B* **2006**, *110*, 8531–8534.
(21) Zheng, J.; Kwak, K.; Xie, J.; Fayer, M. D. *Science* **2006**, *313*, 1951–1955.
(22) Dian, B. C.; Longarte, A.; Mercier, S.; Evans, D. A.; Wales, D. J.; Zwier, T. S. *J. Chem. Phys.* **2002**, *117*, 10688–10702.
(23) Evans, D. A.; Wales, D. J.; Dian, B. C.; Zwier, T. S. *J. Chem. Phys.* **2004**, *120*, 148–157.
(24) Dian, B. C.; Longarte, A.; Winter, P. R.; Zwier, T. S. *J. Chem. Phys.* **2004**, *120*, 133–147.
(25) Bagchi, S.; Kim, Y. S.; Charnley, A. K.; Smith, A. B.; Hochstrasser, R. M. *J. Phys. Chem. B* **2007**, *111*, 3010–3018.
(26) Wang, J.; Zhuang, W.; Mukamel, S.; Hochstrasser, R. *J. Phys. Chem. B* **2008**, *112*, 5930–5937.
(27) Okada, A.; Miura, T.; Takeuchi, H. *Biochemistry* **2001**, *40*, 6053–6060.
(28) Wu, Y.; Voth, G. A. *Biophys. J.* **2005**, *89*, 2402–2411.
(29) Souhassou, M.; Lecomte, C.; Blessing, R. H.; Aubry, A.; Rohmer, M. M.; Wiest, R.; Benard, M.; Marraud, M. *Acta Crystallogr. Sect. B: Struct. Sci.* **1991**, *47*, 253–266.
(30) Asplund, M. C.; Zanni, M. T.; Hochstrasser, R. M. *Proc. Natl. Acad. Sci. U.S.A.* **2000**, *97*, 8219–8224.
(31) Zanni, M. T.; Gnanakaran, S.; Stenger, J.; Hochstrasser, R. M. *J. Phys. Chem. B* **2001**, *105*, 6520–6535.
(32) Kim, Y. S.; Wang, J. P.; Hochstrasser, R. M. *J. Phys. Chem. B* **2005**, *109*, 7511–7521.
(33) Kim, Y. S.; Hochstrasser, R. M. *J. Phys. Chem. B* **2005**, *109*, 6884–6891.
(34) *HyperChem Professional 7.51*; Hypercube, Inc.: Gainesville, FL.
(35) Phillips, J. C. R.; Braun, R.; Wang, W.; Gumbart, J.; Tajkhorshid, E.; Villa, E.; Chipot, C.; Skeel, R. D.; Kalé, L.; Schulten, K. *J. Comput. Chem.* **2005**, *26*, 1781–1802.
(36) Brooks, B. R.; Bruccoleri, R. E.; Olafson, B. D.; States, D. J.; Swaminathan, S.; Karplus, M. *J. Comput. Chem.* **1983**, *4*, 187–217.
(37) Essmann, U.; Perera, L.; Berkowitz, M. L.; Darden, T.; Lee, H.; Pedersen, L. G. *J. Chem. Phys.* **1995**, *103*, 8577–8593.
(38) Mukamel, S. *Principles of Nonlinear Optical Spectrscopy*; Oxford University Press: New York, 1995.
(39) Kwak, K.; Zheng, J. R.; Cang, H.; Fayer, M. D. *J. Phys. Chem. B* **2006**, *110*, 19998–20013.
(40) Hayashi, T.; Mukamel, S. *J. Chem. Phys.* **2006**, *125*.
(41) Oh, K. I.; Han, J.; Lee, K. K.; Hahn, S.; Han, H.; Cho, M. *J. Phys. Chem. A* **2006**, *110*, 13355–13365.
(42) Zhuang, W.; Abramavicius, D.; Hayashi, T.; Mukamel, S. *J. Phys. Chem. B* **2006**, *110*, 3362–3374.
(43) Luzar, A.; Chandler, D. *Phys. Rev. Lett.* **1996**, *76*, 928 LP-931.
(44) Chandra, A. *Phys. Rev. Lett.* **2000**, *85*, 768 LP-771.
(45) Laage, D.; Hynes, J. T. *Science* **2006**, *311*, 832–835.
(46) Schroder, C.; Rudas, T.; Boresch, S.; Steinhauser, O. *J. Chem. Phys.* **2006**, *124*.

JP811168X